High-Capacity Sol−Gel Synthesis of $LiNi_xCo_yMn_{1-x-y}O_2$ ($0 \le x, y \le 0.5$) Cathode Material for Use in Lithium Rechargeable Batteries

C. Nithya, R. Thirunakaran, A. Sivashanmugam, G. V. M. Kiruthika, and S. Gopukumar*

Central Electrochemical Research Institute, Karaikudi, Tamilnadu, India 630 006

Received: July 22, 2009; Revised Manuscript Received: August 28, 2009

Succinic acid assisted sol−gel synthesized layered $LiNi_xCo_yMn_{1-x-y}O_2$ ($0 \le x, y \le 0.5$) materials have been studied as cathode materials for lithium rechargeable batteries. TG/DTA studies were performed on the gel precursor and suggest the formation of a layered phase around 400 °C. The gel precursor was calcined at 850 °C and characterized by means of X-ray diffraction and FT-IR analyses and reveals that all of the synthesized materials are found to be well-crystallized with an α-$NaFeO_2$ layered structure. The effect of Co content on the surface morphology has been examined by scanning electron microscopy, and X-ray photoelectron spectroscopy studies indicate that the oxidation states of nickel, cobalt, and manganese are +2, +3, and +4, respectively. The electrochemical galvanostatic charge/discharge cycling behavior of the synthesized layered materials has been evaluated in the voltage range of 2.7−4.8 V at C/10 and C/5 rates using a 2016 coin-type cell using 1 M $LiPF_6$ in 1:1 EC/DEC as electrolyte. $LiCo_{0.1}Ni_{0.4}Mn_{0.5}O_2$ cathode material delivered the highest average discharge capacity of ~175 mAh/g at a C/10 rate, corresponding to a current density of 0.298 mA cm^{-2} over the investigated 50 cycles.

Introduction

The lithium transition-metal oxides, $LiMO_2$ (M = Co, Ni, and Mn) have been extensively investigated as cathode materials for lithium rechargeable batteries as they possess a unique two-dimensional crystal structure suitable for fast conduction of interlayer lithium ions.[1,2] Among them, $LiCoO_2$ is the most preferred in the majority of commercial lithium ion cells due to its high reversibility and ease of synthesis.[3] However, considering from the economic and environmental view points, the high cost and toxicity of cobalt have led to considerable research efforts toward developing lithium manganate as an alternative cathode.[4] $LiMnO_2$ is thermodynamically unstable in the layered structure. The Mn^{3+} (d^4) ions cause a cooperative distortion of the MnO_6 octahedra due to Jahn−Teller stabilization, leading to a phase transformation to the spinel-like phase, which leads to eventual degradation of electrode performance.[5]

In the present case, numerous attempts have been made to improve the structural stability of this oxide, which reveal that the partial substitution of manganese ions with other transition-metal ions, such as Ni^{2+}, is quite effective in improving the cycleability of $LiMO_2$ cathode material.[6] However, it has some problems to be overcome in order to apply it commercially, such as low tapping density[7,8] and poor rate capability.[9] Generally, alien metal ion doping can effectively improve the electrochemical properties of the cathode material.[10] Regarding layered $LiNi_{0.5}Mn_{0.5}O_2$, many studies have been carried out on the structural and electrochemical properties of the equivalent substituted $LiNi_{0.5}Mn_{0.5}O_2$, such as $LiNi_{0.5}Mn_{0.5-x}Ti_xO_2$ and $LiNi_{0.5-x}Mn_{0.5-x}Co_{2x}O_2$.[11,12] D'Epifanio et al. reported that partial Co substitution for Ni in $LiNiO_2$ effectively improved the electrochemical properties with higher capacity and better cycleability.[13]

The synthesis methods of cathode materials strongly influence their electrochemical behaviors. Compared with solid-state methods, soft methods have many merits and the sol−gel technique is one of the effective methods for the synthesis of cathode material.[14] In this work, we report for the first time the physical (TG/DTA, XRD, SEM, FT-IR, and XPS) and electrochemical (galvanostatic cycling) properties of layered $LiNi_xCo_yMn_{1-x-y}O_2$ synthesized by the sol−gel technique using succinic acid as a chelating agent.

Experimental Section

Synthesis of $LiNi_xCo_yMn_{1-x-y}O_2$ Materials. The $LiNi_xCo_yMn_{1-x-y}O_2$ ($0 \le x, y \le 0.5$) materials have been prepared by the sol−gel method using stoichiometric amounts of lithium, cobalt, nickel, and manganese acetates dissolved in triply distilled water. This mixed solution is then added to succinic acid in the desired proportion and then stirred for 3 h to ensure that the reaction reagents have been uniformly mixed. The aqueous solution of the chelating agent and the metal acetate salts was then evaporated to obtain the gel precursor. The gel precursor containing metal succinates was dried in a vacuum oven for 2 h at 120 °C. Finally, the gel precursor was calcined at 850 °C for 5 h in air atmosphere for obtaining phase pure $LiNi_xCo_yMn_{1-x-y}O_2$ ($0 \le x, y \le 0.5$) materials (see Scheme 1).

Characterization. Thermal analysis (TG/DTA) of the gel precursor has been carried out using a thermal analyzer (PL Thermal Sciences instrument model STA 1500) at a heating rate of 10 °C/min from 10 to 850 °C in air. The structure of the calcined powders has been evaluated with an X-ray diffractometer (X'Pert PRO PANalytical PW 3040/60 X'Pert PRO) using Cu Kα radiation by measuring the diffraction angle (2θ) between 10° and 80° with an increment of 1°/min. Samples for surface morphology have been palletized and examined in a scanning electron microscope (SEM HITACHI S-3000 H, Japan), and images were recorded at 25 kV using a secondary electron detector. The Fourier transform infrared spectrum was recorded on a Nicolet 5DX-FTIR spectroscope using a KBr pellet in the range of 400−2000 cm^{-1}. X-ray photoelectron spectroscopy of the synthesized powder has been investigated using VG electron

* To whom correspondence should be addressed. E-mail: deepika_41@rediffmail.com. Fax: +91-4565-227779.

10.1021/jp907036a CCC: $40.75
Published on Web 09/18/2009

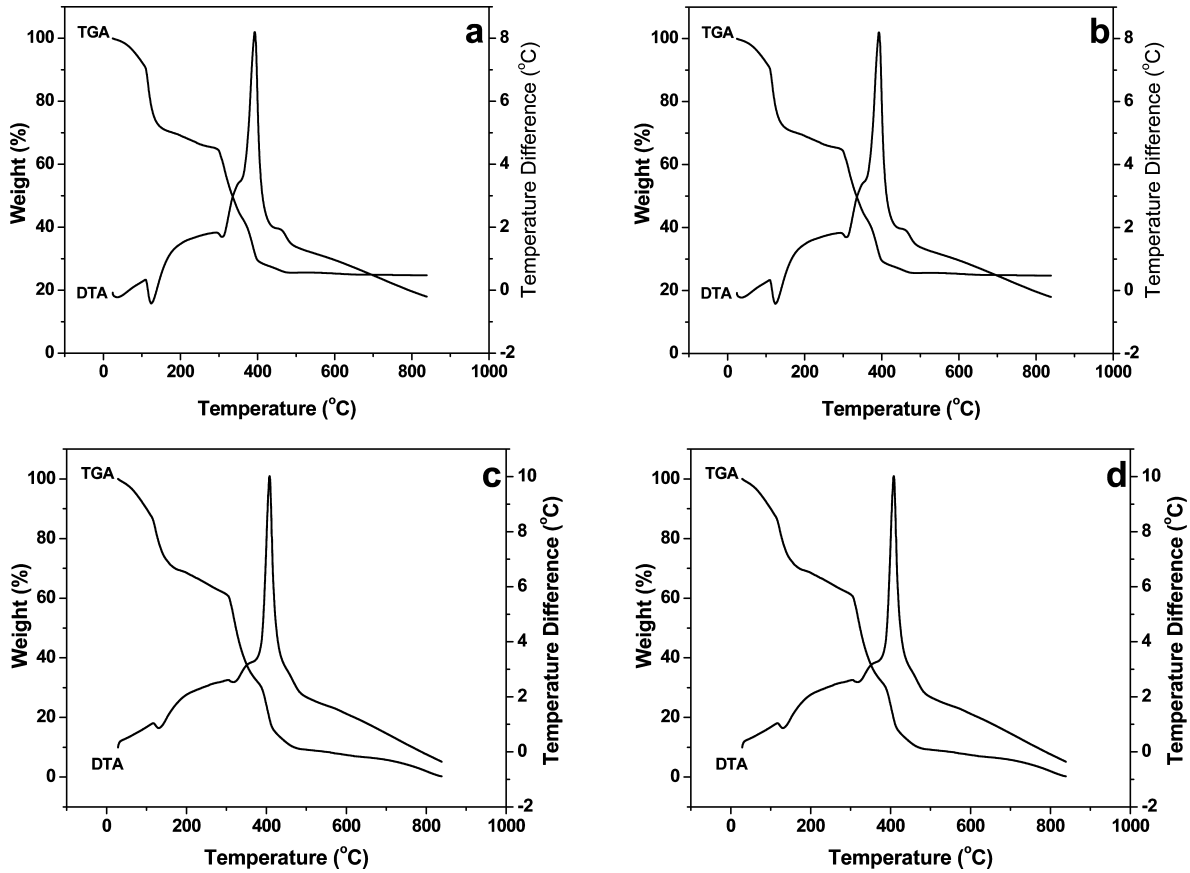

Figure 1. TG/DTA analysis of layered $LiNi_xCo_yMn_{1-x-y}O_2$ precursors: (a) $x, y = 0.5, 0$; (b) $x, y = 0.4, 0.1$; (c) $x, y = 0.25, 0.25$; and (d) x, y = 0.1, 0.4.

SCHEME 1: Flow Chart for the Synthesis of Layered $LiNi_xCo_yMn_{1-x-y}O_2$ ($0 \leq x, y \leq 0.5$) by the Sol−Gel Method Using Succinic Acid as a Chelating Agent

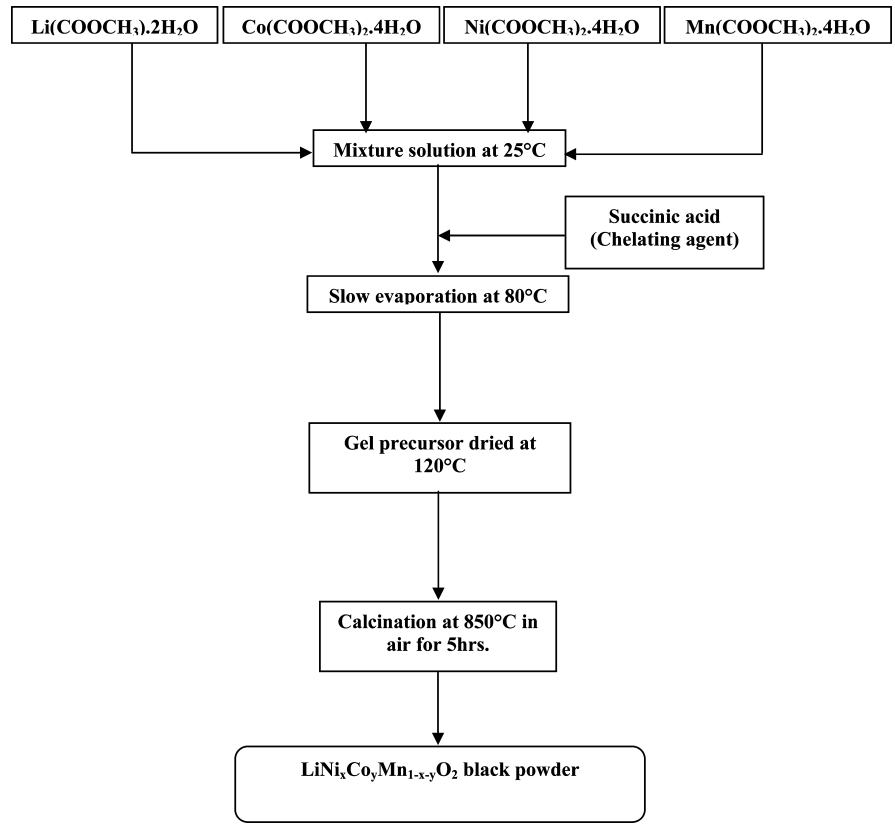

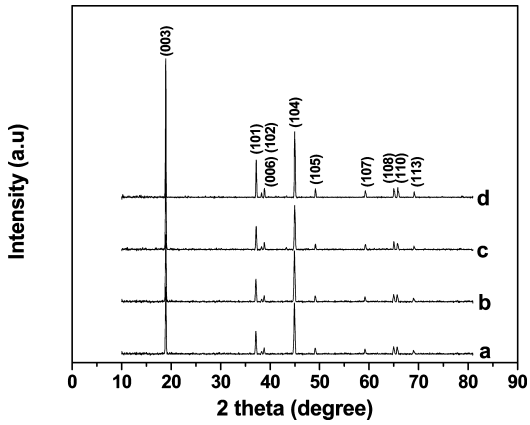

Figure 2. XRD patterns of $LiNi_xCo_yMn_{1-x-y}O_2$ samples calcined at 850°C: (a) $x, y = 0.5, 0$; (b) $x, y = 0.4, 0.1$; (c) $x, y = 0.25, 0.25$; and (d) $x, y = 0.1, 0.4$.

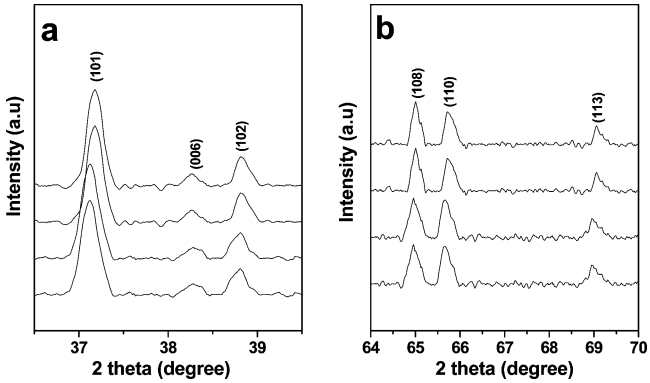

Figure 3. Magnified XRD peaks of (a) (006) and (102) and (b) (108) and (110).

spectroscopy. The powder sample is pressed into pellets and affixed to the sample holder. All spectra were recorded using an X-ray source (Al Kα radiation) with a scan range of 0−1200 eV binding energy. The collected high-resolution XPS spectra were analyzed using the XPS peak fitting software program. The energy scale have been adjusted on the carbon peak (C 1s) spectra at 284.5 eV.

Electrochemical Measurements. Electrochemical measurements have been carried out using a two-electrode 2016 type coin cell assembled in an argon-filled glovebox with metallic lithium as counter and reference electrodes, while the working electrode consists of the synthesized layered $LiNi_xCo_yMn_{1-x-y}O_2$ powder mixture coated onto an aluminum foil current collector. The powder mix in the working electrode consisted of 80% $LiNi_xCo_yMn_{1-x-y}O_2$, 10% acetylene black, and 10% PVDF binder blended with NMP solvent. Celgard 2400 has been used as the separator, and the electrolyte consisted of 1 M $LiPF_6$ with ethylene carbonate and diethylene carbonate (1:1 v/v). The charge−discharge measurements have been carried out on the assembled coin cell using a programmable battery tester in the potential range of 2.7−4.8 V at C/10 and C/5 current rates, corresponding to current densities of 0.298 and 0.597 mA cm^{-2}, respectively.

Results and Discussion

TG/DTA Studies. The TG/DTA profiles for the $LiNi_xCo_yMn_{1-x-y}O_2$ gel precursor materials for varying compositions of x and y in the range from 0 to 0.5 are presented in Figure 1. It can be clearly seen from the curves that the formation of $LiNi_xCo_yMn_{1-x-y}O_2$ materials takes place around 400 °C. There is very little change in the profiles as the Co content is increased from 0 to 0.4. Formation of $LiNi_xCo_yMn_{1-x-y}O_2$ from the precursor stage can be divided into three main regions. The weight loss region from room temper-

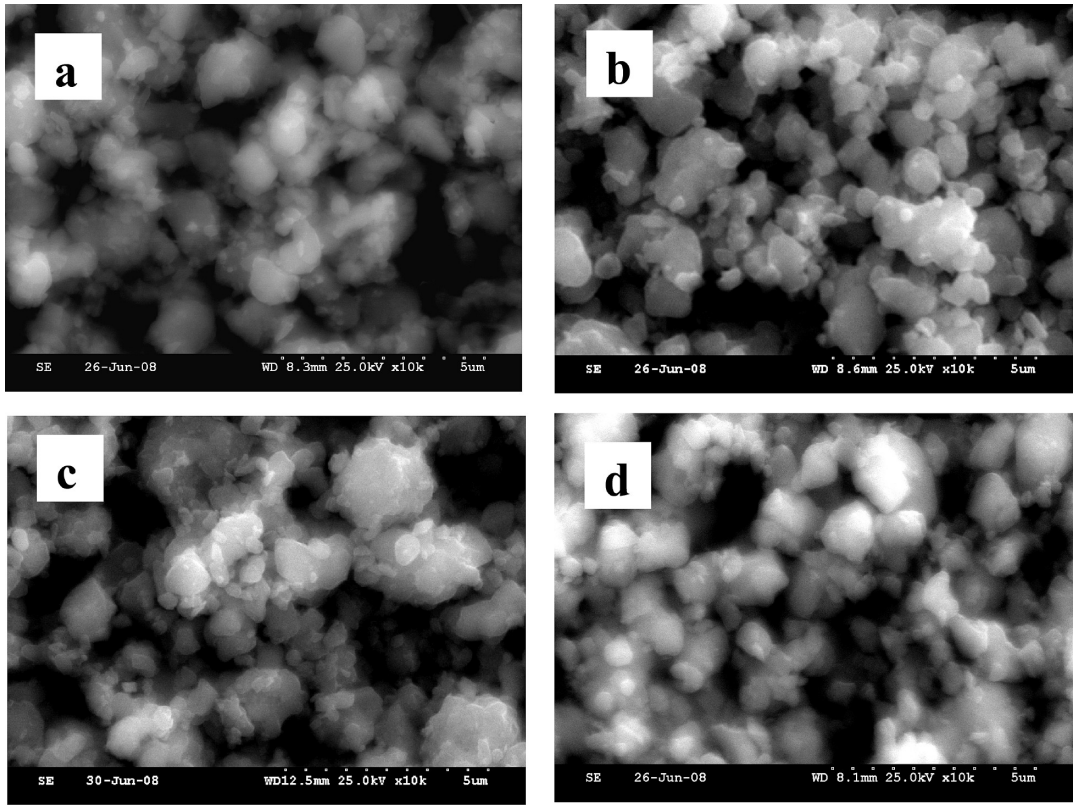

Figure 4. SEM images of $LiNi_xCo_yMn_{1-x-y}O_2$ materials: (a) $x, y = 0.5, 0$; (b) $x, y = 0.4, 0.1$; (c) $x, y = 0.25, 0.25$; and (d) $x, y = 0.1, 0.4$.

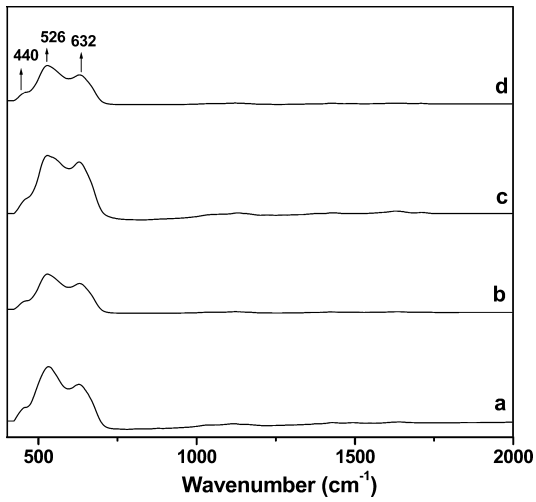

Figure 5. FT-IR spectra of $LiNi_xCo_yMn_{1-x-y}O_2$ materials: (a) $x, y = 0.5, 0$; (b) $x, y = 0.4, 0.1$; (c) $x, y = 0.25, 0.25$; and (d) $x, y = 0.1, 0.4$.

ature to 150 °C can be assigned to loss of water adsorbed on the surfaces and some intercalated water molecules. Thereafter, a slight decrease in weight loss observed between 150 and 300 °C could be due to the initiation of the succinic acid decomposition reaction. A vigorous chemical reaction between 300 and 450 °C, accompanied by about a 50% weight loss, is ascribed to the decomposition of acetate precursors. More than half of the weight loss occurs during this stage because of a violent oxidation−decomposition reaction and formation of the oxide material takes place. The above observations are complemented by the DTA studies, viz., the presence of a strong exothermic peak at 405 °C, corresponding to a 50% weight loss in TGA for the acetate decomposition reaction. However, beyond this temperature, there is no weight loss or reactions involved, indicating the formation of the black powder of $LiNi_xCo_yMn_{1-x-y}O_2$ in the amorphous state.

X-ray Diffraction. XRD patterns of succinic acid assisted sol−gel synthesized $LiNi_xCo_yMn_{1-x-y}O_2$ materials calcined at 850 °C for 5 h in air atmosphere are presented in Figure 2 and show a strong Bragg peak located at ~2 theta (θ) = 18.99° and also medium intensity Bragg peaks located at around 36° and 44°. As evident from Figure 3, all the XRD patterns could be indexed to the α-$NaFeO_2$ structure and match well with the fingerprint peaks, viz., 003, 101, 006, 102, 104, 108, and 110. The observed peak splitting at (006)/(102) and (108)/(110) and the corresponding XRD patterns are magnified in Figure 3. The peaks are clearly split, indicating the formation of a well-ordered α-$NaFeO_2$-type layered structure. The ratio of the intensities of 003 and 104 is greater than unity, suggesting no cation mixing in the layered structures. R-value refers to the ratio of the sum diffraction intensity of (006) and (102) to the diffraction intensity of (101), which scales the cation disorder, which is minimum for $x = 0.1$. Manthiram et al.[15] reported that the lower cation disordered sample has a larger thickness of the interslab space for lithium, that is, d(LiO_2), which can lead to an easier diffusion or extraction of the lithium ions. Lattice parameters of the samples have been calculated by a unit cell package software and are presented in Table 1. It is interesting to note that, with increasing Co content in the samples, the "*a*" and "*c*" constants and unit volume decreased monotonically. Stoyanova[16] reported that the small size of a dopant contracts the lattice volume for a solid-solution system. The ionic radii of Ni^{2+} and Co^{3+} ions are 0.76 and 0.53 A°,[17] respectively. The increase in the content of Co^{3+} ion in the Mn site correspondingly decreases the Ni^{2+} ion content, resulting in shrinkage in the lattice volume. Furthermore, the *c*/*a* ratio of all the materials is observed to be above 4.94 for all samples, thereby suggesting improved layered characteristics, and therefore, the ions should exhibit excellent electrochemical behavior.

Scanning Electron Microscopy. The surface morphology of the synthesized materials has been investigated using SEM and is presented in Figure 4. The particles are larger for the composition of x, $y = 0.5, 0$ as compared with cobalt-doped samples. Further, the particles of $LiNi_{0.25}Co_{0.25}Mn_{0.5}O_2$ and $LiNi_{0.1}Co_{0.4}Mn_{0.5}O_2$ are present as larger grains of average particle size ranging from 0.4 to 1 μm with agglomeration. It is interesting to note that the morphology of the $LiNi_{0.4}Co_{0.1}Mn_{0.5}O_2$ sample orients into a smaller particle size of 0.2 μm. Such a kind of reduction in particle size indicates that the insertion or extraction of lithium ions could easily take place due to reduction in diffusion path lengths, thereby enhancing the electrochemical activity.

Vibrational Spectra. The local environments of cations in a cubic close packed oxygen array of the $LiNi_xCo_yMn_{1-x-y}O_2$ lattices were investigated by using FT-IR spectroscopy, and the results are presented in Figure 5. An IR mode corresponds to vibrations involving primarily atomic motion of cations against their oxygen neighbors. Layered oxides, such as $LiMO_2$, possess a crystal structure consisting of alternating layers of trigonally distorted LiO_6 and MO_6 octahedra sharing edges. The transition-metal cations (i.e., Co, Ni, Mn) and lithium ions are located at Wychoff sites 3*a* and 3*b*, respectively.[18] The Li^+ and Co^{3+}/Ni^{2+}/Mn^{4+} ions are ordered along the (111) direction of the rock-salt cubic lattice, leading to a two-dimensional structure.[19] Thus, the IR absorption bands for $LiNi_xCo_yMn_{1-x-y}O_2$ powders are explained as three absorption bands whose center is located at 440, 526, and 632 cm^{-1}. The high frequency bands of the FT-IR absorption spectra of $LiNi_xCo_yMn_{1-x-y}O_2$ located at 632 cm^{-1} are attributed to the asymmetric stretching modes of the MO_6 group, whereas the low-frequency bands at 440 and 556 cm^{-1} are allocated to the O−M−O bending vibration.[20] It is curious to observe that an increase in cobalt content shifts the frequency to the higher wavenumber region. This is due to cationic disorder in $Ni_xCo_yMn_{1-x-y}O_2$ ($x = 0.25, 0.1$ and $y = 0.25, 0.4$) slabs, which is in good agreement with the XRD observation. The broadening of high wavenumber IR bands may be related with the inhomogeneous distribution of Ni/Co/Mn and the vibration in cation−anion bond lengths and/or polyhedral distortion occurring in $LiNi_xCo_yMn_{1-x-y}O_2$.[21]

X-ray Photoelectron Spectroscopy Studies. $LiNi_xCo_yMn_{1-x-y}O_2$ materials were characterized by XPS to confirm the oxidation states of the transition-metal ions. Figure 6 presents the XPS spectra of C 1s, Li 1s, Co 2p, Ni 2p, Mn

TABLE 1: Unit Cell Parameters and Crystallite Size of $LiNi_xCo_yMn_{1-x-y}O_2$ ($0 \le x, y \le 0.5$) Materials

x, *y*	*a* (A°)	*c* (A°)	*c*/*a*	cell volume $(A°)^3$	I_{003}/I_{004}	*R*	crystallite size (nm)
0.5, 0	2.893	14.327	4.952	104.732	1.89	0.52	120.7
0.4, 0.1	2.892	14.310	4.948	104.319	1.78	0.47	59.2
0.25, 0.25	2.892	14.298	4.943	103.918	1.63	0.49	100.8
0.1, 0.4	2.891	14.290	4.942	103.450	1.25	0.57	112.4

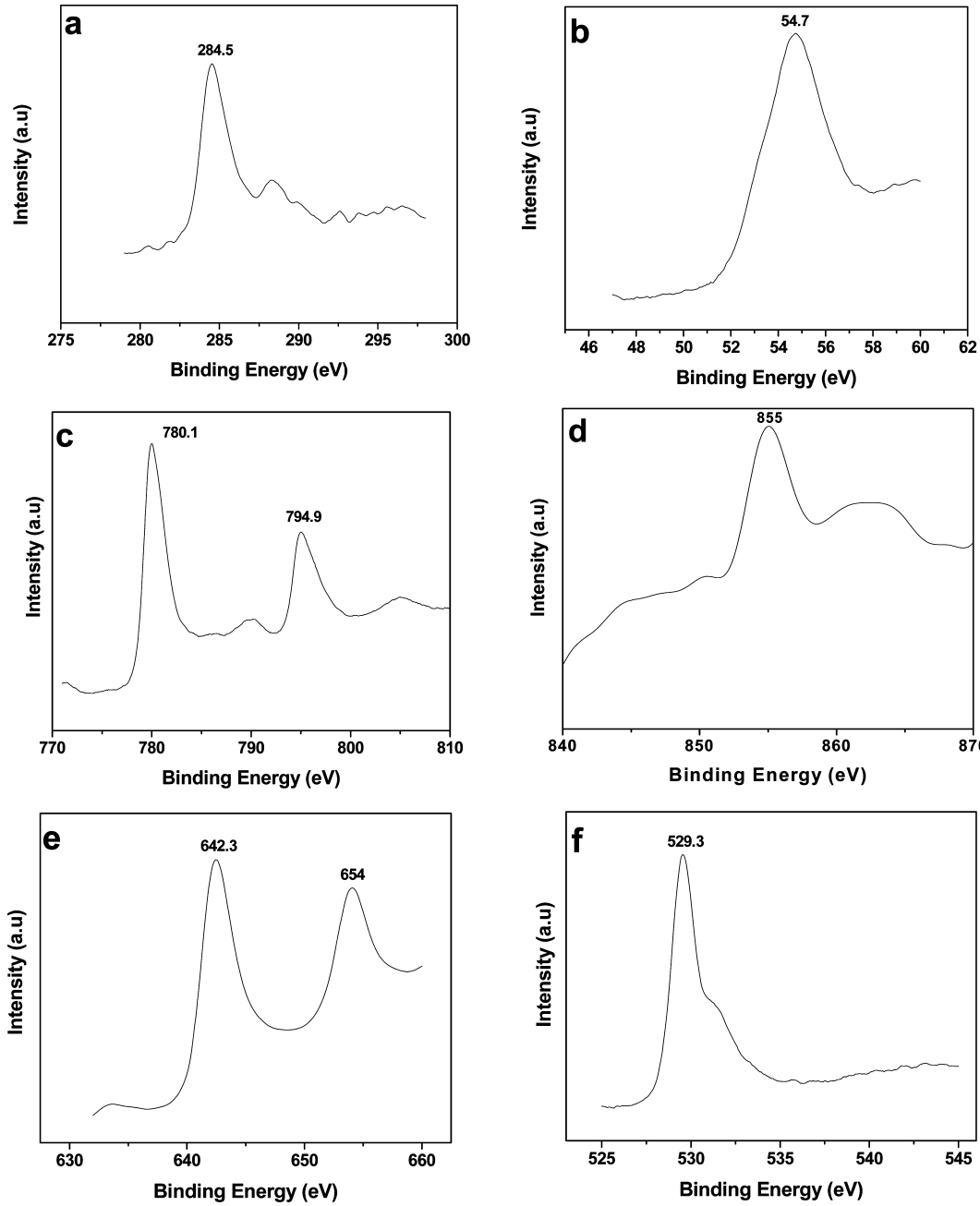

Figure 6. X-ray photoelectron spectroscopy of $LiCo_{0.1}Ni_{0.4}Mn_{0.5}O_2$ materials: (a) C 1s, (b) Li 1s, (c) Co 2p, (d) Ni 2p, (e) Mn 2p, and (f) O 1s.

2p, and O 1s components of $LiNi_{0.4}Co_{0.1}Mn_{0.5}O_2$. The C 1s emission peak is observed around 284.5 eV, which is used as the reference in the present XPS measurements. The BE of the Li 1s emission peak is located at 54.7 eV and appears as a broad signal. This value is slightly lower than that reported for Li_2O[22] and suggests, as expected, through ionization of lithium atoms in the layered compounds. The Co 2p XPS spectrum shows a well-defined profile with the $2p_{3/2}$ and $2p_{1/2}$ components at 780.1 and 794.9 eV. A satellite peak is clearly distinguished as an additional peak of low intensity at 9.7 eV, higher in binding energy than the main components. This result suggests that the valence of cobalt is trivalent state, well-consistent with those reported by Shaju[23] and Madhavi et al.[24] The Ni XPS spectrum reveals the characteristic binding energy located around at 855 eV with a satellite peak at 861 eV; hence, it could be assigned to Ni^{2+}. The presence of the satellite peak has also been observed by other researchers and has been ascribed to the multiple splitting of the nickel oxide energy levels.[25,26] This value is somewhat slightly higher than that reported for other Ni-based layered compounds ($LiNi_{0.5}Ti_{0.5}O_2$, 854.1 eV), as reported by Yuncheng et al.,[27] and also well-consistent with Ni in NiO.[28] XPS spectra of the $Mn2p_{3/2}$ component have a main peak at 642.3 eV, which can be indexed to the Mn^{4+}, while the satellite peak is observed located at the BE value of 654 eV in the synthesized $LiNi_{0.4}Co_{0.1}Mn_{0.5}O_2$. This value is in close agreement with previously reported results.[29] O 1s spectra showed an interesting evolution with the preparation method. The BE value of the O 1s component is located at 529.3 eV, originating from Ni−O, Mn−O, and Co−O in the synthesized material. From the above-obtained results, we could say that binding energies located at 780.1, 854.7, and 642.3 eV are due to the presence of Co in +3, Ni in +2, and Mn in +4 states, respectively.

Charge−Discharge Studies. Figure 7 shows the initial charge−discharge curves of the $LiNi_xCo_yMn_{1-x-y}O_2$ materials

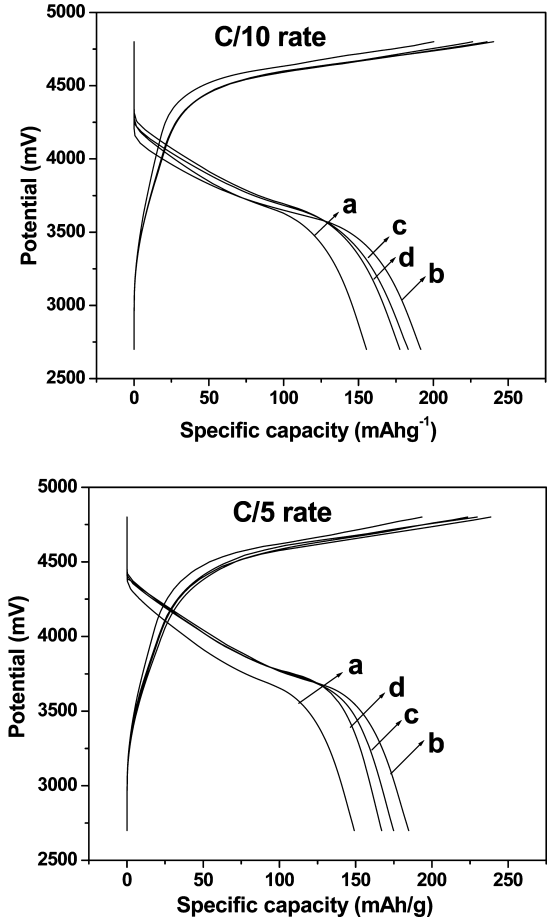

Figure 7. Charge−discharge behavior of $LiNi_xCo_yMn_{1-x-y}O_2$ materials: (a) x, $y = 0.5$, 0; (b) x, $y = 0.4$, 0.1; (c) x, $y = 0.25$, 0.25; and (d) x, $y = 0.1$, 0.4.

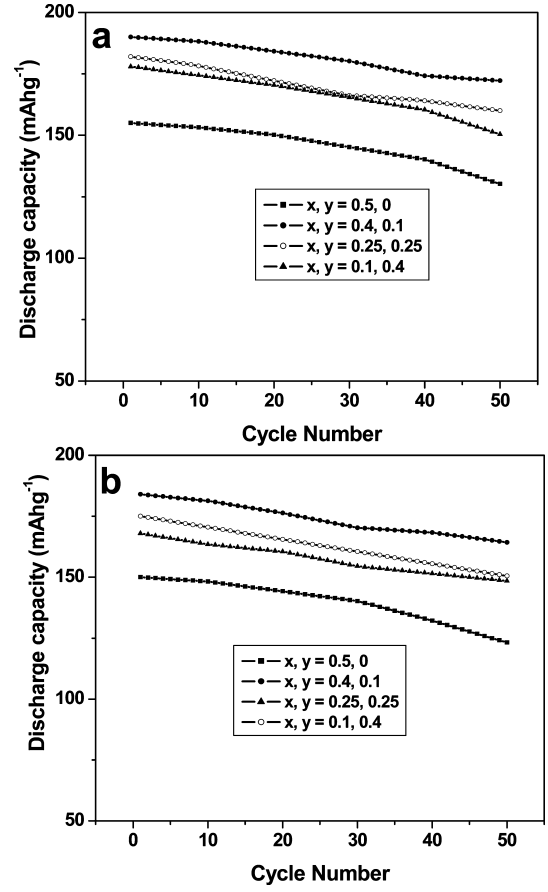

Figure 8. Cycling performance of $LiNi_xCo_yMn_{1-x-y}O_2$ materials: (a) C/10 rate and (b) C/5 rate.

cycled from 2.7 to 4.8 V at C/10 and C/5 current rates, corresponding to current densities of 0.298 and 0.597 mA cm^{-2}, respectively. All samples are the same in terms of the shape of their charge/discharge curves, and no new plateau is observed; there is no evidence of a double plateau around 4 V. It is known that, typically, a double plateau appears in the discharge curves of layered manganese oxides as their structure changes to spinel-related phase.[30] Hence, the absence of such a peak around 4 V indicates that spinel-related phases are not formed. On the other hand, discharge curves are smooth, indicating that the presence of manganese leads to an oxide network favorable for good lithium intercalation. The initial discharge capacities of the samples x, $y = (0.5, 0)$, (0.4, 0.1), (0.25, 0.25), and (0.1, 0.4) are 155, 190, 182, and 178 at the C/10 rate. It is noted that decrease in the cobalt content enhances the discharge capacities. The polarization of the cells declines when the Ni content increases, hence charge-transfer resistance also decreases. Furthermore, the higher content of nickel increases both the initial charge and the discharge capacities and decreases the irreversible capacity, as illustrated in Table 2. However, when the cobalt content is over to 0.25, both the initial charge and the discharge capacities decrease slightly and irreversible capacity slightly increases. This is attributed to the reduction in Ni^{2+} content as well as the larger particle size for $y = 0.4$.

Figure 8 depicts the capacities of the synthesized $LiNi_xCo_yMn_{1-x-y}O_2$ materials calcined at 850 °C over the investigated 50 cycles at C/10 and C/5 current rates, corresponding to current densities of 0.298 and 0.597 mA cm^{-2}, respectively. It can be seen that the composition with x, $y = 0.5$, 0, that is, $LiNi_{0.5}Mn_{0.5}O_2$, exhibits the charge and discharge capacities of 200 and 155 mAh/g, respectively, for the first cycle at a current rate of C/10 in the voltage range of 2.7−4.8 V. At the end of the 50th cycle, 130 mAh/g is obtained; 84% of the initial capacity is retained. The obtained values of capacity for $LiNi_{0.5}Mn_{0.5}O_2$ are in good agreement with literature reports.[6,31] The 1st and 50th cycle discharge capacities of all the samples are presented in Table 2. With increasing current rate, the discharge capacities are slightly decreased, which is attributed to the increase of cell polarization, leading to the decrease of average discharge potential.[32] $LiNi_{0.5}Mn_{0.5}O_2$ samples exhibit poor cycling performance compared with cobalt-doped samples due to the large change in unit cell volume during the charge and discharge cycling.[33] Cobalt and nickel doping should bring about a high mixed conductivity. The increase in polarization observed at the end of discharge is the result of reintercalation difficulty caused by low ionic conductivity when most of the available sites are occupied. Cobalt and nickel substitution can lead to a decrease in the nonstoichiometric character of lithium manganate, which favors the cycling characteristics. However, when the amount of Co reaches 0.4, the decrease in the capacities of the active materials is rather substantial. This is probably due to the decrease in Li ion mobility caused by disintegration of the crystal structure. Figure 9 shows the charge/discharge capacities of the 1st, 10th, 20th, 30th, 40th, and 50th cycles of $LiNi_{0.4}Co_{0.1}Mn_{0.5}O_2$ cathode material at current densities of 0.298 and 0.597 mA cm^{-2}. The very low irreversible capacity (37.8 mAh g^{-1}) observed for the present samples when cycled up to 4.8 V is superior as compared with ~50 mAh g^{-1}

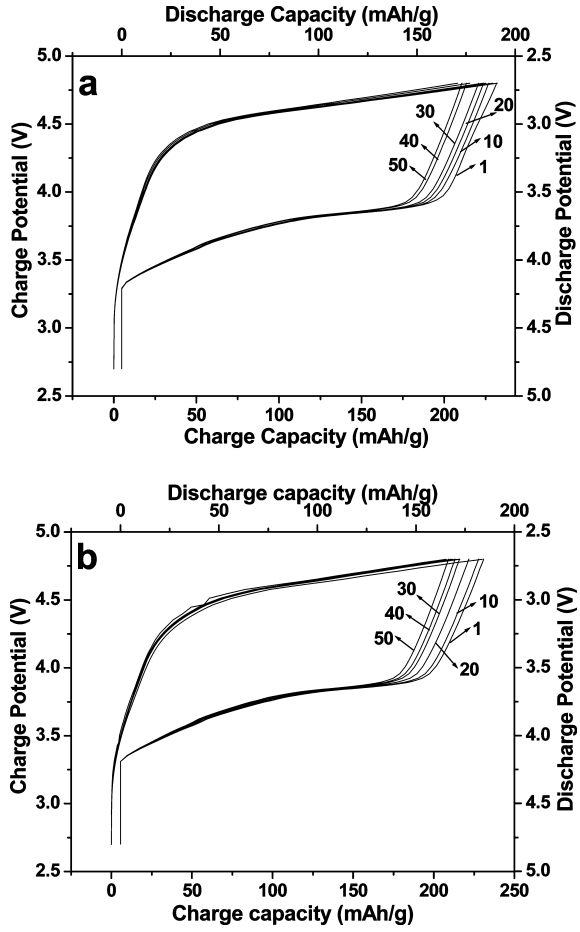

Figure 9. Charge−discharge profiles of the $LiNi_{0.4}Co_{0.1}Mn_{0.5}O_2$ material: (a) C/10 rate (current density = 0.298 mA cm^{-2}) and (b) C/5 rate (current density = 0.597 mA cm^{-2}).

for $LiNi_{0.45}Mn_{0.45}Co_{0.1}O_2$[34] and $LiMn_{0.4}Ni_{0.4}Co_{0.2}O_2$[32] synthesized by coprecipitation mixed hydroxide methods. Table 2 compares the cycling performance of sol−gel synthesized Ni- and Co-doped $LiMnO_2$ materials using citric acid and succinic acid (in the present case) as chelating agents. The good cycling performance observed in the present case is due to the greater complex-forming tendency of suucinic acid than other carboxylic acids.[40] Furthermore, the dissociability of a carboxylic acid depends upon its pK_a values (4.21 for succinic acid and 3.15 for citric acid); the dissociability increases as the chain length decreases. Thereby, carboxylic group ionization and subsequent bonding with the cations may be expected to become stronger and it also shows best hexagonal ordering. On comparison of the reports of the previous researchers, the Ni- and Co-doped $LiMnO_2$ materials synthesized by the sol−gel method using succinic acid as chelating agent in the present case and cycled up to 4.8 V exhibit less capacity fade (9% over the investigated 50 cycles), demonstrating superior cycling performance for these materials synthesized by various other methods.[32,41−47]

Differential Capacity Studies. Figure 10 shows the differential capacity vs potential curves of $LiNi_xCo_yMn_{1-x-y}O_2$ over the potential range of 2.6−4.8 V at C/10 and C/5 rates. The peaks in the dQ/dV curves of all samples correspond to the plateaus in the voltage profile of the charge and discharge curves, as can be seen in Figure 7. As we observe no peak around 3 V, it can be said that no manganese is present in the +3 state[48] in the synthesized materials. It is clear from the figures that the major oxidation and reduction peaks are observed at around 4.6 and 3.8 V, respectively, and is representative of lithium deintercalation and reintercalation processes, respectively. These peaks are also the signature of the hexagonal phase in these types of layered compounds. These observed peaks could be assigned to the Ni^{2+}/Ni^{4+} electrochemical process. Arachi et al.[49] reported that the Ni^{2+}/Ni^{4+} oxidation peak presents at 4.35 V, which is cycled between 2.7 and 4.6 V. In the present work,

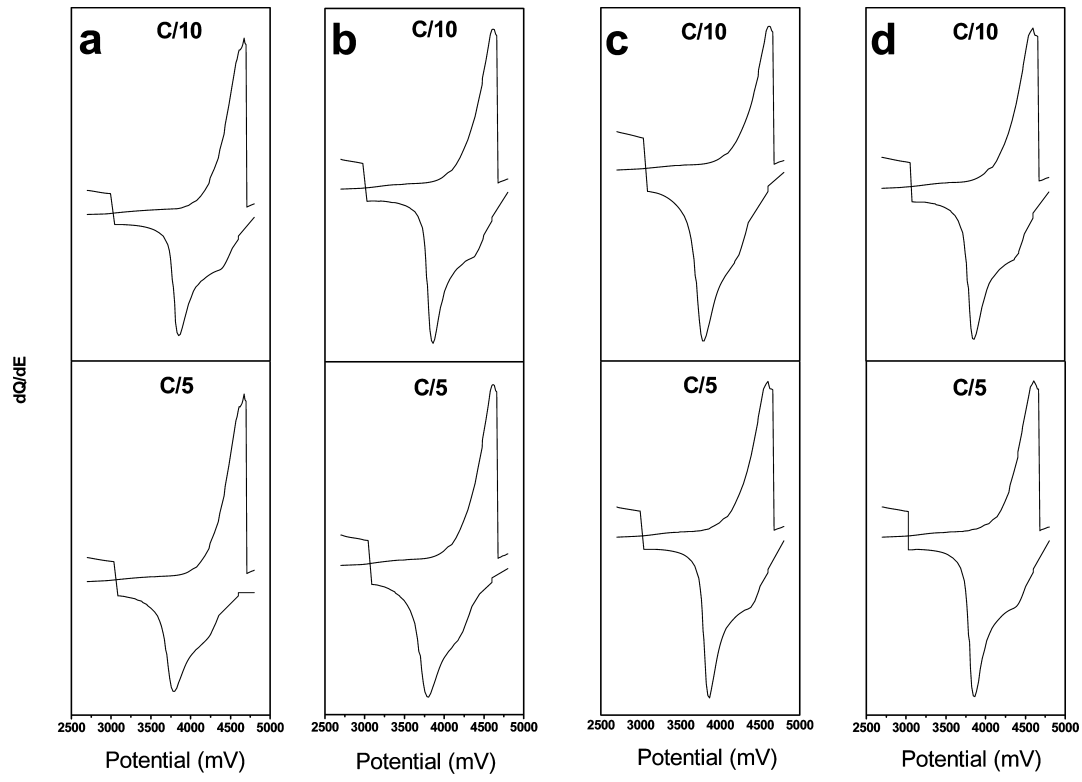

Figure 10. Differential capacity curves of $LiNi_xCo_yMn_{1-x-y}O_2$ materials: (a) x, y = 0.5, 0; (b) x, y = 0.4, 0.1; (c) x, y = 0.25, 0.25; and (d) x, y = 0.1, 0.4.

TABLE 2: Cycling Performances of Co- and Ni-Doped $LiMnO_2$ Synthesized by Using Citric Acid and Succinic Acid as Chelating Agents

cathode material	chelating agent	discharge capacity (mAh/g)		capacity fade (%)	current rate/density	potential range (V)
		1st cycle	n^{th} cycle			
$LiNi_{0.7}Co_{0.25}Mn_{0.05}O_2$	citric acid[35]	189	175(30)	7.4	C/5	3.0−4.3
$LiNi_{0.3}Co_{0.6}Mn_{0.1}O_2$	citric acid[36]	142.3			0.1 mA/cm^2	2.2−4.2
$LiNi_{1-x-y}Co_xMn_yO_2$	citric acid[37]	198	182(20)	16.3	C/10	3.0−4.5
$LiNi_xCo_{1-2x}Mn_xO_2$	citric acid[38]	192	185(20)	3.3	C/10	3.0−4.5
$LiNi_{0.33}Co_{0.33}Mn_{0.33}O_2$	citric acid[39]	211.8	∼160(50)	24	20 mAh/g	2.9−4.6
$LiNi_{0.4}Co_{0.1}Mn_{0.5}O_2$	succinic acid	190	174(50)	9	C/10	2.7−4.8
		184	164(50)	10	C/5	2.7−4.8
$LiNi_{0.25}Co_{0.25}Mn_{0.5}O_2$	succinic acid	182	160(50)	12	C/10	2.7−4.8
		175	151(50)	14	C/5	2.7−4.8
$LiNi_{0.1}Co_{0.4}Mn_{0.5}O_2$	succinic acid	178	150(50)	15	C/10	2.7−4.8
		168	141(50)	16	C/5	2.7−4.8

the upper cutoff voltage has been raised up to 4.8 V and the Ni^{2+}/Ni^{4+} oxidation peak shifts to 4.55 V, which is in good agreement with Song et al.[42] According to Lu and Dahn,[50] this shift arises due to the removal of electrons from the oxygen atom in the structure. On the other hand, no oxidation peak of Mn^{3+} to Mn^{4+} could be observed in the charging process, which partially proves that the prepared sample contains only Mn^{4+} and is not involved in the redox process. These results are in accordance with those reported earlier.[42,51] From the above investigations, it is clearly understood that Co dopant is an attractive candidate to enhance the electrochemical performance of $LiNi_{0.5}Mn_{0.5}O_2$ material.

Conclusions

Layered $LiNi_xCo_yMn_{1-x-y}O_2$ ($0 \le x, y \le 0.5$) materials have been synthesized for the first time by the sol−gel method using succinic acid as chelating agent. All samples have a phase-pure layered structure with a space group of *R*3*m*. It seems that the presence of cobalt ($x < 4$) leads to an oxide network favorable for good lithium insertion and deinsertion. Excessive Co content results in shrinkage in the lattice volume and slightly increases the cation disorder. XPS studies suggest that Ni, Co, and Mn are present in +2, +3, and +4 oxidation states, respectively. The $LiCo_{0.1}Ni_{0.4}Mn_{0.5}O_2$ material demonstrates good cycling performance in the voltage range of 2.7−4.8 V with a good capacity retention of ∼175 and ∼170 mAh/g at C/10 and C/5 rates, respectively, over the investigated 50 cycles.

Acknowledgment. The authors thank the Department of Science and Technology, India, for support under the DST-JST project GAP12/08.

References and Notes

(1) Zou, M.; Yoshio, M.; Gopukumar, S.; Yamaki, J. *Chem. Mater.* **2003**, *15*, 4699.
(2) Julien, C.; Gastro-Garcia, S. *J. Power Sources* **2001**, *97*−*98*, 943.
(3) Julien, C.; Camacho-Lopez, M.; Lemal, M.; Mohan, T.; Chitra, S.; Kalyani, P.; Gopukumar, S. *Solid State Ionics* **2000**, *135*, 241.
(4) Sulochana, A.; Thirunakaran, R.; Sivashanmugam, A.; Gopukumar, S.; Yamaki, J. *J. Electrochem. Soc.* **2008**, *155*, A206.
(5) Vitins, G.; West, K. R. *J. Electrochem. Soc.* **1997**, *144*, 2587.
(6) Gopukumar, S.; Chung, K. Y.; Kim, K. B. *Electrochim. Acta* **2004**, *49*, 803.
(7) Li, D.; Muta, T.; Noguchi, H. *J. Power Sources* **2004**, *135*, 262.
(8) Jouanneau, S.; Dahn, J. R. *J. Electrochem. Soc.* **2004**, *151*, A1749.
(9) Cushing, B. L.; Goodenough, J. B. *Solid State Sci.* **2002**, *4*, 1487.
(10) Zou, M.; Yoshio, M.; Gopukumar, S.; Yamaki, J. *Chem. Mater.* **2005**, *17*, 1284.
(11) Li, D.; Noguchi, H.; Yoshio, M. *Electrochim. Acta* **2004**, *50*, 425.
(12) Sun, Y.; Ouyang, C.; Wang, Z.; Huang, X.; Chen, L. *J. Electrochem. Soc.* **2004**, *151*, A504.
(13) D'Enfanio, A.; Croce, F.; Ronci, F.; Rossi Albertinc, V.; Traversa, E.; Scrosati, B. *Chem. Mater.* **2004**, *16*, 3559.
(14) Zaheena, C. N.; Nithya, C.; Thirunakaran, R.; Sivashanmugam, A.; Gopukumar, S. *Electrochim. Acta* **2009**, *54*, 2877.
(15) Venkatraman, S.; Choi, J.; Manthiram, A. *Electrochem. Commun.* **2004**, *6*, 832.
(16) Stoyanova, R.; Zhicheva, E.; Alcantara, R.; Tirado, J. L.; Bromiley, G.; Bromiley, F.; Ballaran, T. B. *J. Mater. Chem.* **2004**, *14*, 366.
(17) Shannon, R. D. *Acta Crystallogr., Sect. A: Cryst. Phys. Diffr. Theor. Gen. Crystallogr.* **1976**, *32*, 756.
(18) Gopukumar, S.; Jeong, Y.; Kim, K. B. *Solid State Ionics* **2003**, *159*, 223.
(19) Julien, C.; Letranchant, C.; Rangan, S.; Lemal, M.; Ziolkiewicz, S.; Castro-Garia, S.; El-Farh, L.; Benkaddour, M. *Mater. Sci. Eng.* **2000**, *76*, 145.
(20) Rougier, A.; Nazri, G. A.; Julien, C. *Ionics* **1997**, *3*, 170.
(21) Nazri, M.; Curtis, D.; Yebka, B.; Nazri, G. A.; Julien, C. *Extended Abstracts of 193rd Meeting of The Electrochemical Society*, San Diego, CA, May 3−8, 1998, Vol. 98−1.
(22) Kanamura, K.; Tamura, H.; Shiraishi, S.; Takehara, J. *J. Electrochem. Soc.* **1995**, *142*, 340.
(23) Shaju, K. M.; Subba Rao, G. V.; Chowdari, B. V. R. *Electrochim. Acta* **2002**, *48*, 145.
(24) Madhavi, S.; Subba Rao, G. V.; Chowdari, B. V. R.; Li, S. F. Y. *J. Electrochem. Soc.* **2001**, *148*, A1279.
(25) Carley, A. F.; Jackson, S. D.; O'Shea, J. N.; Roberts, M. W. *Surf. Sci.* **1999**, *440*, L868.
(26) Amine, K.; Tukamato, H.; Yasuda, H.; Fujita, Y. *J. Electrochem. Soc.* **1996**, *143*, 1607.
(27) Sun, Y.; Wang, Z.; Huang, X.; Chan, L. *J. Power Sources* **2005**, *146*, 678.
(28) Wagner, C. D.; Riggis, W. M.; Davis, L. E.; Moulder, J. F.; Mullenberg, G. E. *Handbook of X-ray Photoelectron Spectroscopy*; Perkin-Elmer Corporation: Eden Prairie, MN, 1979.
(29) Kang, S. H.; Kim, J.; Stoll, M. E.; Abraham, D.; Sun, Y. K.; Amine, K. *J. Power Sources* **2002**, *112*, 41.
(30) Ammundsen, A.; Paulsen, J. *Adv. Mater.* **2001**, *13*, 943.
(31) Abdel-Ghany, A.; Zaghib, K.; Gendron, F.; Mauger, A.; Julien, C. M. *Electrochim. Acta* **2007**, *52*, 4092.
(32) Ma, M.; Chernova, N. A.; Toby, B. H.; Zavalij, P. Y.; Wittingham, M. S. *J. Power Sources* **2007**, *165*, 517.
(33) Ueda, A.; Ohzuku, T. *J. Electrochem. Soc.* **1994**, *141*, 2013.
(34) Xiao, J.; Chernova, N. A.; Whittingham, M. S. *Chem. Mater.* **2008**, *20*, 7454.
(35) Li, X.; Kang, F.; Shen, W.; Bai, X. *J. Phys. Chem. Solids* **2008**, *69*, 1246.
(36) Hernandez, A.; Fabela, S.; Carlos, L.; Gonzalez, T.; Sanchez, E. *Ceram. Int.* **2008**, *34*, 225.
(37) Hwang, B. J.; Tsai, Y. W.; Chen, C. H.; Santhanam, R. *J. Mater. Chem.* **2003**, *13*, 1962.
(38) Chen, C. H.; Wang, C. J.; Hwang, B. J. *J. Power Sources* **2005**, *146*, 626.
(39) Wen, Z.; Hanxing, L.; Chen, H.; Xianjun, Z.; Yanxi, L. *Rare Met.* **2008**, *27*, 158.
(40) Azab, H. A.; El-Nady, A. M.; Hassan, A.; Azkal, R. S. A. *Monatsh. Chem.* **1993**, *124*, 637.
(41) Kosova, N. V.; Devyatkina, E. T.; Kaichev, V. V. *J. Power Sources* **2007**, *174*, 965.
(42) Song, C. H.; Stephan, A. M.; Lee, Y. S.; Nahm, K. S. *Mater. Chem. Phys.* **2007**, *101*, 63.
(43) Kim, J. M.; Chung, H. T. *Electrochim. Acta* **2004**, *49*, 3573.

(44) Lee, K. S.; Myung, S. T.; Sun, Y. K. *Chem. Mater.* **2007**, *19*, 2727.

(45) Li, D.; Saski, Y.; Kobayakawa, K.; Sato, Y. *Electrochim. Acta* **2006**, *51*, 3809.

(46) Sun, Y. K.; Myung, S. T.; Shin, H. S.; Bae, Y. C.; Yoon, C. S. *J. Phys. Chem. B* **2006**, *110*, 6810.

(47) Liao, P. Y.; Dun, J. G.; Sheen, S. R. *J. Power Sources* **2005**, *143*, 212.

(48) Paulsen, J. M.; Thomas, C. L.; Dahn, J. R. *J. Electrochem. Soc.* **2000**, *147*, 861.

(49) Arachi, Y.; Kobayashi, H.; Emura, S.; Nakata, Y.; Tanaka, M.; Asai, T. *Chem. Lett.* **2003**, *32*, 60.

(50) Lu, Z.; Dahn, J. R. *J. Electrochem. Soc.* **2002**, *149*, A815.

(51) Park, S. H.; Sun, Y. K. *J. Power Sources* **2003**, *119*−*121*, 161.

JP907036A